3. Isobutanol Synthesis at High Pressure in CMRU

A $Cu_{0.5}Mg_5O_x$ catalyst was examined in the synthesis of isobutanol from CO/H_2 at 593 K and 4.5 MPa and space velocities between 6000-1000 cm^3 (STP)/ g-cat.h. The results are presented in Figure 11a and Table 6. As a comparison, the results obtained on K-$Cu_{0.5}Mg_5CeO_x$ (MG3-11Ow/K) are also given in Figure 11b and Table 6.

CO conversion on $Cu_{0.5}Mg_5O_x$ increases with increasing bed residence time; methanol is the major product followed by paraffins, isopropanol, ethanol, and propanol. CO conversion rates decrease with increasing bed residence time, suggesting a gradual approach to methanol synthesis equilibrium. Methanol selectivity decreases and isobutanol selectivity increases with increasing bed residence time, suggesting that methanol is a reaction intermediate that undergoes further reactions at longer bed residence times leading to higher alcohols, such as isobutanol. $Cu_{0.5}Mg_5O_x$ catalysts show high hydrocarbon and low isobutanol selectivities compared to K-$Cu_{0.5}Mg_5CeO_x$, consistent with the lower basicity of the K-free catalyst. The $^{13}CO_2/^{12}CO_2$ isotopic exchange results indicate that a greater number of basic sites are available on K-$Cu_{0.5}Mg_5CeO_x$ compared to $Cu_{0.5}Mg_5O_x$ (Table 7). Moreover, the strength of these available basic sites are stronger on K-$Cu_{0.5}Mg_5CeO_x$. Strong basic sites lead to higher isobutanol production rates. Isobutanol production increases with increasing bed residence time, suggesting 1) isobutanol is a secondary reaction product and 2) CO_2, one of the reaction product, does not inhibit isobutanol formation on $Cu_{0.5}Mg_5O_x$ as strongly as on K-$Cu_{0.5}Mg_5CeO_x$ because of the weaker basicity of the former. Methanol turnover rates on $Cu_{0.5}Mg_5O_x$ (7.0×10^{-3} CH_3OH/surface Cu.s) are higher than on K-$Cu_{0.5}Mg_5CeO_x$ (4.6×10^{-3} CH_3OH/surface Cu.s), suggesting that the active site (Cu) for methanol synthesis on K-$Cu_{0.5}Mg_5CeO_x$ is inhibited by reaction products such as CO_2 and H_2O. The Cu atoms in K-$Cu_{0.5}Mg_5CeO_x$ are more likely to be oxidized by CO_2 and/or H_2O because of the small Cu crystallites (Table 7) and strong interaction between Cu and CeO_x.

As mentioned earlier, a large batch of 1.0 wt % K-$Cu_{0.5}Mg_5CeO_x$ catalyst has been prepared recently. This catalyst will be tested again for the synthesis of isobutanol from CO/H_2 and used in future studies of alcohol-chain growth reactions. This run will consist of 1) variation in space velocity, 2) addition of 1-propanol, 3) addition of ethanol, 4) addition of CO_2, and 5) changes in reaction temperatures. The gas chromatograph TCD and FID will also be recalibrated using a mixture containing Ar, He, N_2, CO, CO_2, methane, ethane, ethylene, propane, propylene, acetylene, methanol, ethanol, and DME.

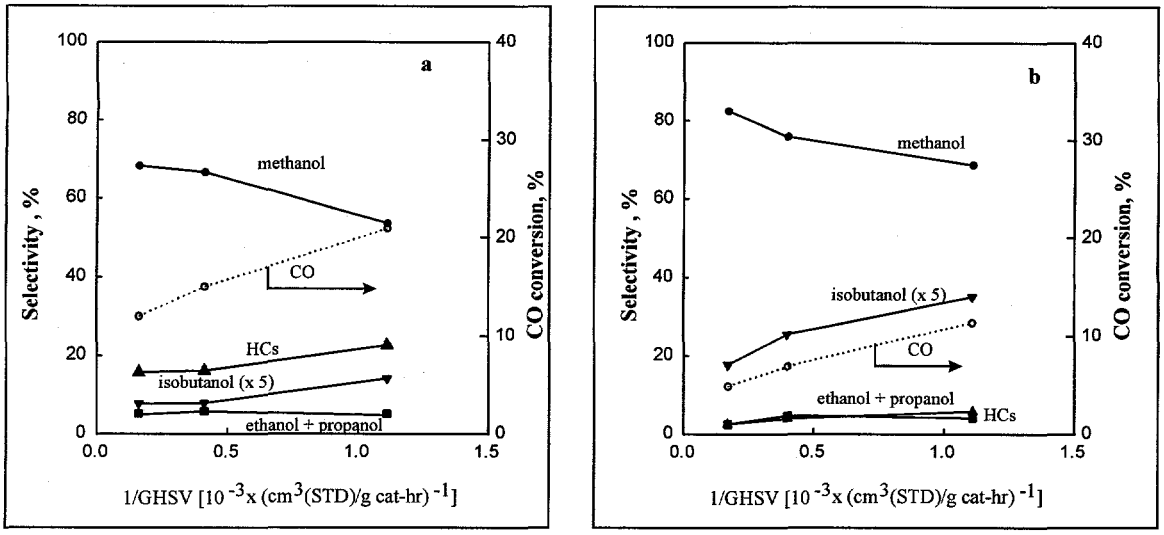

Figure 11. CO conversion and product selectivities vs. space velocity on a) $Cu_{0.5}Mg_5O_x$ and b) 1.1 wt % K-$Cu_{0.5}Mg_5CeO_x$. (593 K, 4.5 MPa, CO/H_2 =1).

Table 6. Product selectivities and methanol turnover rates on $Cu_{0.5}Mg_5O_x$ (CMRU-22) and K-$Cu_{0.5}Mg_5CeO_x$ (CMRU-20).

Catalyst	$Cu_{0.5}Mg_5O_x$	$Cu_{0.5}$ Mg_5O_x	K-$Cu_{0.5}Mg_5CeO_x$
GHSV [cm^3/g cat. h]	903	6262	903
CO conversion [%]	20.9	12.0	11.4
Methanol turnover rate [$mol_{Methanol}/mol_{Surface\ Cu\text{-}S}$]	7.0	37.2	4.6
Product selectivities [%]			
Methanol	53.6	68.3	68.7
Ethanol+propanol	5.1	5.1	4.1
isobutanol	2.8	1.6	7.0
CO_2	18.8	12.3	22.3
Paraffins	22.6	15.8	5.8

Reaction conditions: 593 K, 4.5 MPa, H_2/CO=1, 2.06 g catalyst.

Task 4: Identification of Reaction Intermediates

4.1. Determination of Copper Surface Area

The decomposition of N_2O has been used to measure Cu surface areas on K-$CuMgCeO_x$ catalysts. All these catalysts have been pre-reduced at 623 K in 5 % H_2/He. The decomposition of N_2O on reduced ZnO support sites has been found to contribute significantly to the overall Cu surface area on Cu/ZnO catalysts [12]. It is possible that the decomposition of N_2O on the reduced CeO_x species in pre-reduced $CuMgCeO_x$ catalysts also corrupts N_2O titration and leads to overestimates of copper dispersion. Our previous studies have shown that N_2O is not consumed on Cu-free $MgCeO_x$ samples pre-reduced at 623 K, suggesting that CeO_x remains in its full oxidation state during H_2 treatment. This observation, however, cannot rule out the possibility that CeO_2 may

reduce when Cu is available to dissociate H_2 in Cu-containing $MgCeO_x$ samples. In effect, the presence of Cu may promote the reduction of CeO_2.

In order to rule out any contributions from reduced CeO_x species to N_2O titration measurements of Cu surface area, a reduction-oxidation cycle was performed. A $Cu_{0.5}Mg_5CeO_x$ sample was reduced at 623 K and N_2O titration data at 363 K were obtained. The measured Cu surface area was found to be 19.0 m^2/g-cat (23 % Cu dispersion). This sample was re-reduced at 473 K instead of 623 K. Surface oxygen atoms on Cu surface can be removed at 473 K in H_2, but reduction of CeO_2 is likely to occur only at much higher reduction temperatures. Thus, reduction at 473 K is likely to remove oxygen from Cu surface but not from CeO_x. The Cu area of the sample reduced at 473 K was 19.3 m^2/g-cat, which is very similar to the value of 19.0 m^2/g-cat obtained on the fresh sample after reduction at 623 K. This demonstrates that CeO_x does not contribute to the measured copper dispersion and that these high dispersion values indeed reflect the presence of small Cu metal crystallites (about 5 nm). An additional exposure of this titrated sample to 5 % H_2/He at 423 K resulted in a Cu surface area of 17.9 m^2/g-cat, suggesting that oxygen atoms chemisorbed on Cu can be almost completely removed by H_2 at temperatures as low as 423 K.

4.2. Determination of Basic Site Density and Strength

The density and strength of basic sites were measured from the exchange capacity and rates obtained in a $^{13}CO_2/^{12}CO_2$ isotopic exchange method developed as part of this project; this method provides a direct measure of the number of basic sites *"kinetically available" at reaction temperatures*. In addition, this technique provides a measure of the distribution of reactivity among available basic sites. In this method, a pre-reduced catalyst (50 mg) is exposed to a 0.1 % $^{13}CO_2$/0.1 % Ar/He stream (100 cm^3/min) and after $^{13}CO_2$ reached a constant level in the effluent, the flow is switched to 0.1 % $^{12}CO_2$/He (100 cm^3/min). The relaxation of the $^{13}CO_2$ displaced from the surface is followed by mass spectrometry. In contrast with CO_2 temperature programmed desorption (TPD), $^{13}CO_2/^{12}CO_2$ exchange methods probe the density and reactivity of reactive basic sites at reaction temperatures and chemical equilibrium, without contributions from unreactive carbonates and without disrupting the steady-state coverage on catalytic solids.

Figure 12 shows the transients obtained on a $Cu_{0.5}Mg_5CeO_x$ catalysts when the isotopic composition of CO_2 was switched at 573K. As $^{13}CO_2$ was switched to $^{12}CO_2$ at zero time, without altering the partial pressure or flow rate of CO_2, the concentration of $^{13}CO_2$ decreases as $^{12}CO_2$ concentration increases and the total gas phase concentration of CO_2 (i.e., $^{12}CO_2 + {}^{13}CO_2$) remains constant. The presence of Ar as an inert tracer permits correction for gas holdup and hydrodynamic delay in the apparatus.

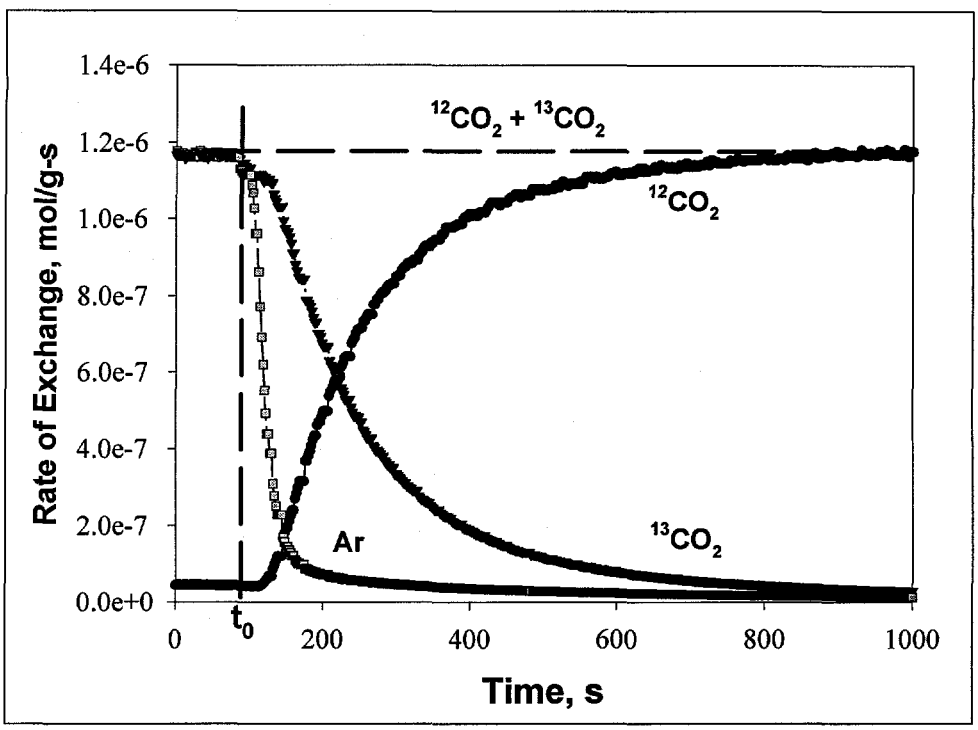

Figure 12. Steady-state transients observed for $Cu_{0.5}Mg_5CeO_x$ upon switching from $^{13}CO_2$/He to $^{12}CO_2/H_2$ at 573 K.

The significant delay in the steady-state transient of $^{13}CO_2$, relative to Ar curve, indicates that the former originates from catalyst-bound $^{13}CO_2$ species that desorb slowly at the temperature of the isotopic exchange experiment. The coverage or number of surface CO_2 species remains constant, i.e.,

$$\theta_{^{13}CO_2\,(t=0)} = \theta_{^{13}CO_2\,(t)} + \theta_{^{12}CO_2\,(t)} = \theta^{total}_{CO_2\,(t)} = \theta_{^{12}CO_2\,(t=\infty)}$$

At $t=t_0$, the surface is only covered by $^{13}CO_2$ and at a longer time after the switch, the surface is predominantly occupied by $^{12}CO_2$. Therefore, the amount of $^{13}CO_2$ displaced from the surface by $^{12}CO_2$ reflects the exchange capacity of the catalyst at the reaction temperature. The exchange capacity is determined from the area under the $^{13}CO_2$ curve (Figure 12). This area, properly corrected for the response factor of the mass spectrometer and gas holdup, corresponds to the number of basic sites that participate in exchange reactions at 573 K. The number of basic sites (exchangeable CO_2) kinetically available for exchange experiments on MgO, CeO_2, and K-, CeO_x- and AlO_x- modified MgO samples are shown in Table 7. Weakly interacting sites are mostly unoccupied by CO_2 and strongly interacting sites do not exchange in the time scale of the isotopic relaxation experiment. These strongly interacting sites and weakly interacting sites are also unlikely to contribute to catalytic reactions at similar temperatures.

As a comparison, the number of basic sites determined from CO_2 temperature programmed desorption (TPD) measurements based on the amount of CO_2 released at temperature below 573 K are also given in Table 7. In this method, CO_2 is adsorbed on the pre-reduced catalyst (50 mg) at room temperature for 10 min. The catalyst surface is subsequently flushed with He (100 cm^3/min) to remove gas phase and weakly adsorbed CO_2 before linearly ramping the temperature at 0.5 K/s, and measuring the CO_2 desorption profile by mass spectrometry. The area below the TPD curve was used to measure the number of CO_2 molecules desorbed, and the number of basic sites on the metal oxide surface was calculated using a 1:1 CO_2 / basic site stoichiometry.

Table 7. Composition, surface area, and basic site density of mixed metal oxides

[a]Sample	[b]Sg, m^2/g	[c]Cu, dispersion, %	Exchangeable CO_2 at 300 °C 10^{-6} mol/m^2	CO_2 desorbed during TPD at T < 300 °C 10^{-6} mol/m^2
MgO	191	/	0.38	0.50
CeO_2	80	/	0.92	/
K-Mg_5CeO_x	188	/	0.95	0.84
$Cu_{0.5}Mg_5O_x$	118	6	0.40	/
0.1 wt% K-$Cu_{0.5}Mg_5CeO_x$	167	23	1.20	0.62
1.1 wt% K-$Cu_{0.5}Mg_5CeO_x$	147	14	2.33	0.64
3.5 wt% K-$Cu_{0.5}Mg_5CeO_x$	62	6	5.22	0.65
1.2 wt % K-$Cu_{7.5}Mg_5CeO_x$	92	5	3.17	0.91
Cs-Cu/ZnO/Al_2O_3	62	/	1.09	0.62

[a] Bulk composition measured by atomic absorption.
[b] Total surface area determined by N_2 BET adsorption at 77 K.
[c] Dispersion calculated from the ratio of surface Cu (determined by N_2O decomposition at 90 °C [13, 14]) to the total number of Cu atoms in the catalyst.

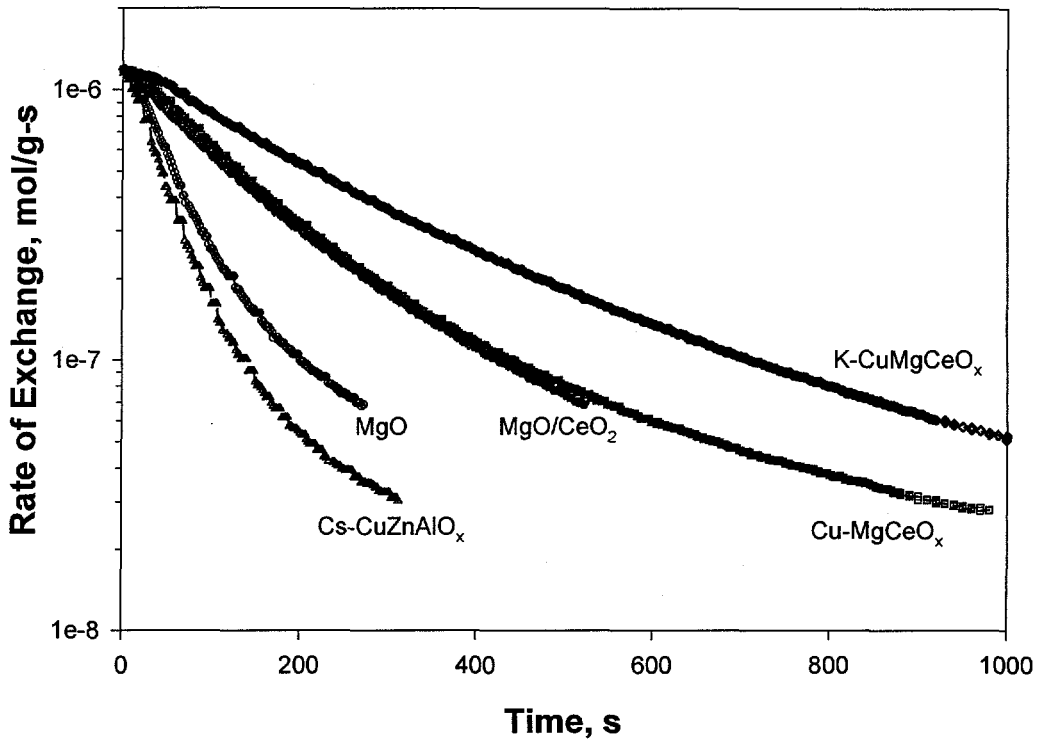

Figure 13. The transient response observed for mixed oxides upon switching from $^{13}CO_2$ to $^{12}CO_2$: T = 573 K.

The local slope in the semi-logarithmic plots of Figure 13 reflects the dynamics of the first-order CO_2 exchange reaction and thus the exchange rate constant on available basic sites. The curved semi-logarithmic plots show that $Cu_{0.5}Mg_5CeO_x$ surfaces contain sites with a broad distribution of exchange rate constants, because uniform surfaces with only one type of adsorption site would lead to linear plots in Figure 13. Exchange rate constants depend on the thermodynamics of binding interactions between CO_2 and basic sites through linear free energy relations commonly used to estimate activation energies for chemical reactions [15]. Large exchange rate constants and the concomitant short relaxation times (*e.g.* on MgO and Cs-Cu/ZnO/Al_2O_3) reflect shorter CO_2 surface lifetimes and weaker binding of CO_2 molecules on available basic sites.

The distribution of exchange rate constants was obtained for each catalyst sample from the relaxation dynamics using inverse Laplace transform deconvolution methods [16]. These distributions of exchange kinetic constants are shown in Figure 14. The distribution curves were normalized to give an area of unity. The y-axis represents the distribution function f(k), where f(k)dk is defined as the fraction of the total number of kinetically accessible basic sites with exchange rate constants between k and k+dk. The logarithmic rate constant in the x-axis of Figure 14 can be related to an activation energy for exchange if we assume that the pre-exponential factors for adsorption-desorption rate constants are not influenced by basic strength:

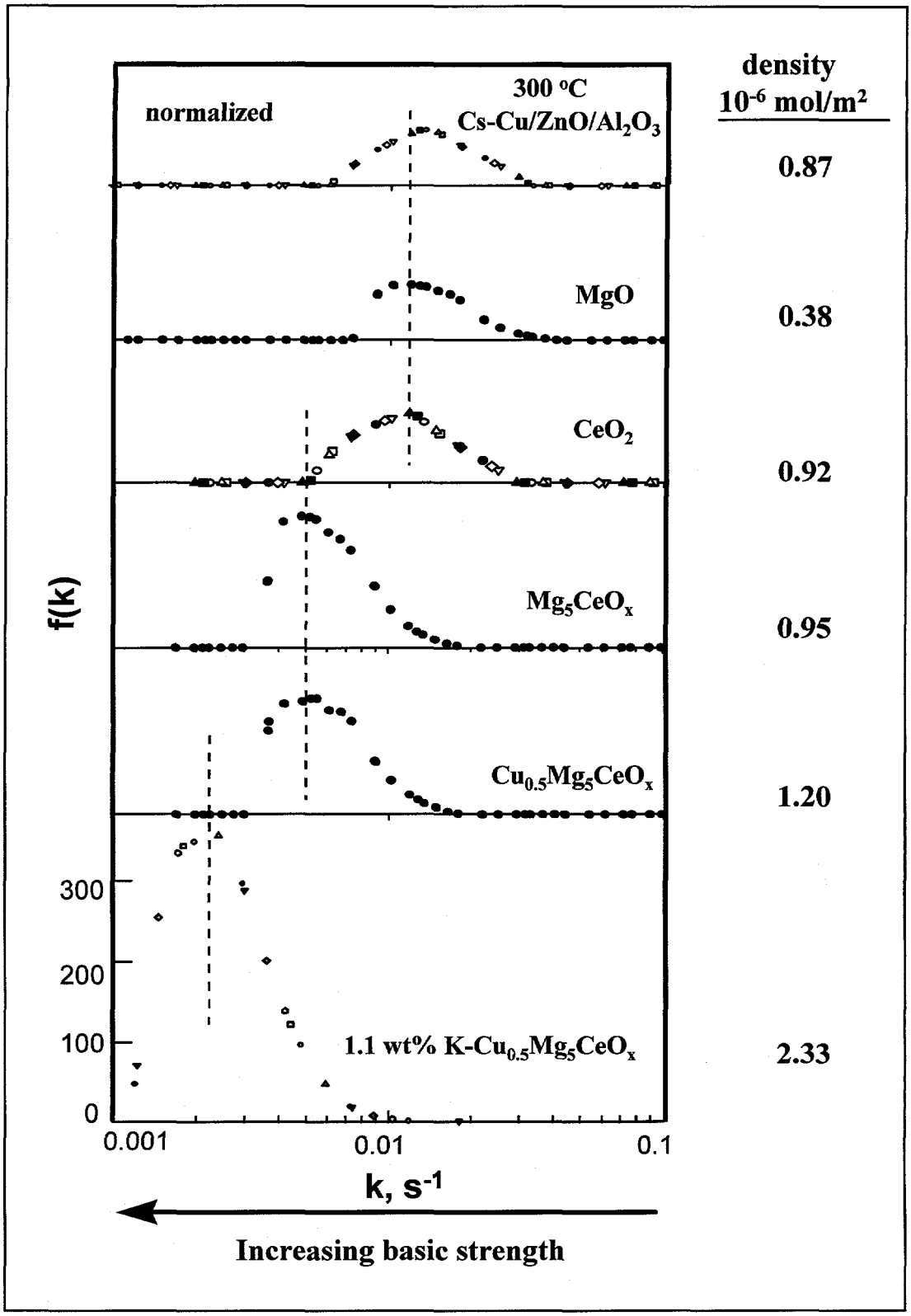

Figure 14. Basic strength distribution with respect to exchange rate constant for mixed metal oxides.

$$\log k = \log [A \exp (-E/RT)] = \log A - (2.3\ E/RT)$$

The use of linear free energy relations between the activation energy and the enthalpy of adsorbed CO_2 :

$$E = E_o - \alpha \Delta H_{ads}$$

preserves the linear dependence between the logarithm of k and the enthalpy of CO_2 adsorption; the latter is directly related to the basic strength of surface sites on MgO-based solids.

As shown in Table 7, the surface density of available basic sites on MgO at 573 K is 0.38 x 10^{-6} mol/m^2. This site density is much lower than the value of 18.3 x 10^{-6} mol/m^2 reported for MgO surface oxygen density [17], and it corresponds to about 2.1 % of these surface lattice oxygen in MgO acting as basic sites available for $^{13}CO_2/^{12}CO_2$ isotopic exchange reaction at 573 K. This number (2.1 %) is lower than the values reported by Davis et al. [17] (25 %) and Kurokawa et al. [18] (10 %) using CO_2 TPD. This is not unexpected since the $^{13}CO_2/^{12}CO_2$ isotopic switch method only probes the number of basic sites that participate in the exchange reactions near 573 K. Weakly basic sites are mostly unoccupied by CO_2 and strongly interacting basic sites do not exchange in the time scale of isotopic exchange experiment. The number of basic sites given by Davis and Kurokawa, however, include both weak and strong basic sites that are not detected by the isotopic exchange method. Neither strong nor weak basic sites are likely to contribute to catalytic reactions at temperatures similar to those of the isotopic switch experiments. The CO_2 TPD results shown in Table 7 do not reflect the total but the number of basic sites that release CO_2 below 573 K. It should be pointed out that the basicity of MgO depends strongly on the source, purity, preparation procedures, and calcination temperatures of MgO [19-21]. All these variables affect the concentrations of surface OH species (less basic) and coordinately unsaturated oxygen (O_{cus}) sites like kinks, steps, corners, and edges.

Basic site densities in CeO_2 determined by either isotopic exchange or CO_2 TPD method are higher than on MgO (Table 7). In fact, the *available basic sites at 573 K* in CeO_2 are stronger compared those in MgO as evidenced by the lower exchange rate constants on CeO_2 (Figure 14). This does not necessarily mean that CeO_2 is a stronger base than MgO, because the stronger basic sites on MgO are not probed by $^{13}CO_2/^{12}CO_2$ exchange experiment at 573 K. $^{13}CO_2/^{12}CO_2$ exchange experiments carried out on a CeO_x sample without 5 % H_2/He reduction at 623 K show a similar density of basic sites and strength compared to the sample subject to H_2 treatment, suggesting that H_2 treatment at 623 K did not affect the properties of available basic sites at 573 K.

The presence of small amounts of CeO_x in MgO (Mg/Ce = 5) increases both the density (Table 7) and strength (Figure 14) of basic sites kinetically accessible for exchange reactions at 573 K. Similar phenomena have been reported by Rane et al. [22] using a CO_2 temperature programmed desorption. These authors observed a marked

increase in the number of both weak and strong basic sites per gram of catalyst upon addition of ceria to MgO. The electron density and consequently the basicity of oxygen ions associated with both Ce^{4+} and Mg^{2+} cations are expected to be different from the ones bounded to only Ce^{4+} or Mg^{2+} ions. As mentioned early, MgO surfaces may have a high density of very strong basic sites that are not probed by $^{13}CO_2/^{12}CO_2$ exchange nor involved in catalytic reactions near 573 K. The presence of Ce^{4+} ions, because of their higher electron affinities compared to Mg^{2+} ions, tend to attract electrons from the oxygen ions associated with Mg^{2+}, resulting in a decrease in *electron* density and basic strength of these oxygen ions and therefore making them available for exchange (and catalysis) at 573 K. The increase in basic site density and strength might also be due to the creation of low-coordinated oxygen ions in the boundary region of these two oxides.

The presence of Cu in $MgCeO_x$ samples slightly increase the basic site density (Table 7) but does not modify the basic strength distribution (Figure 14). Ikawa and co-workers [18] have also reported recently that the distribution of surface basicity on MgO is not modified by the presence of Cu^{2+} ions even though the basic site density increased significantly. They proposed that the larger Cu^{2+} ion is introduced into the MgO lattice, which causes a distortion in the lattice and leads to an increase in the Mg-O bond length and in the localization of electrons near the oxygen ions. In this case, we would expect, however, a change in the distribution of basic site strength. The slightly increase in basic site density in $Cu_{0.5}Mg_5CeO_x$ compared to Mg_5CeO_x may result instead from the contribution of adsorption sites associated with Cu^{2+} ions because Cu metal in the pre-reduced sample could be oxidized by CO_2 during the $^{13}CO_2/^{12}CO_2$ exchange experiment at 573 K. In fact, during CO_2 temperature programmed desorption experiments where Cu is likely to remain metallic, the number of basic sites is lower in $Cu_{0.5}Mg_5CeO_x$ than in Mg_5CeO_x.

The addition of K (1.1 wt %) increases not only the density of basic sites on $Cu_{0.5}Mg_5CeO_x$ (Table 7), but also their strength, as shown by the shift in the distribution to lower exchange rate constants (Figures 14). An increase in K loading from 1.1 to 3.5 wt % increased basic site density from 2.3 to 5.2×10^{-6} m^2/g, but essentially had no effect on the exchange rate constant distribution. Because of the lower electron affinity of K^+ compared to Mg^{2+}, the oxygen ion of K_2O has a higher negative charge, and therefore is more basic than that of MgO. Moreover, the oxygen ions connected with both K^+ and Mg^{2+} ions are expected to have higher electron density compared to ones associated with only Mg^{2+}, resulting in the formation of stronger basic sites in MgO.

Calcination of hydrotalcite (magnesium-aluminum hydroxycarbonate) results in a mixed-oxide solid solution with high surface area and high thermal and hydrothermal stability. This material is active for base-catalyzed reactions, including aldol-condensation and double bond isomerization reactions [23,24]. Stork and co-workers [24] used Hammett indicators and the kinetics of double-bond isomerization to suggest that $MgAlO_x$ oxides exhibit strong basic sites similar to those of pure MgO. McKenzie et al. [17] using temperature-programmed desorption of CO_2 and the decomposition of 2-propanol and Dumesic et al. [25] using microcalorimetric measurement of CO_2 heat of

adsorption suggested that $MgAlO_x$ mixed-metal oxides are less basic than pure MgO. In this study, the basicity of $MgAlO_x$ mixed-metal oxides was measured by using both temperature-programmed desorption of CO_2 and $^{13}CO_2/^{12}CO_2$ isotopic exchange methods and the results are shown in Table 8.

Table 8. Composition, surface area, basic site density of mixed metal oxides

Sample	K, wt %	Surface area (m^2/g)	$^{13}CO_2/^{12}CO_2$ exchange at 573 K $\mu mol/m^2$	$^{13}CO_2/^{12}CO_2$ exchange at 473 K $\mu mol/m^2$	$^{13}CO_2$ TPD at T < 573 K $\mu mol/m^2$	$^{13}CO_2$ TPD T< 723 K $\mu mol/m^2$
$MgAlO_x$	0.08	230	0.21	0.25	0.50	0.66
Mg_3AlO_x	0.02	238	0.17	0.21	0.34	0.50
Mg_5AlO_x	0.02	184	0.10	0.09	0.30	0.41
MgO	/	125	0.35	0.43	1.17	1.50

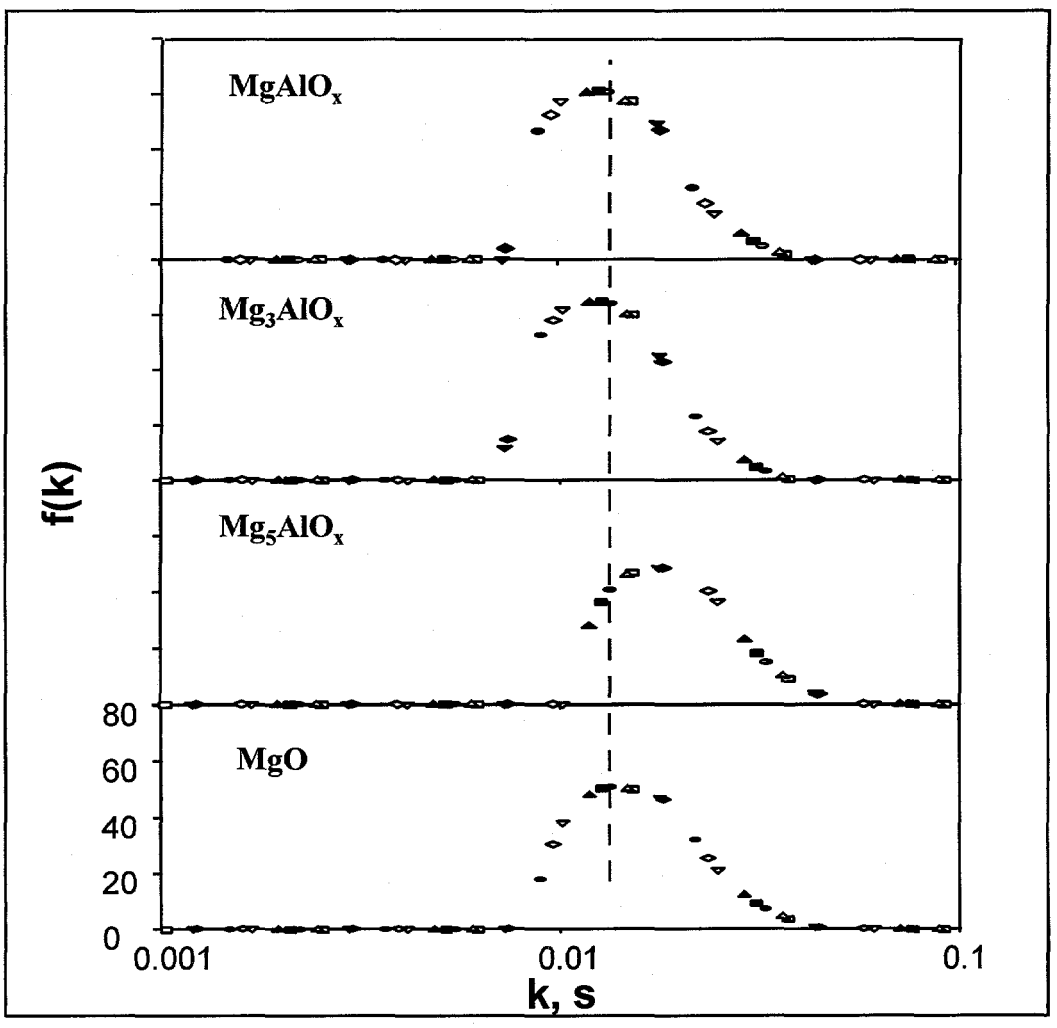

Figure 15. Basic site distribution on pure and Al-modified MgO at 573 K.

The basic site density on MgO determined by the $^{13}CO_2/^{12}CO_2$ exchange method is higher than on any of the $MgAlO_x$ samples (Table 8), suggesting that the addition of Al to MgO decreases the number of basic sites kinetically available at 573 K. The distributions of basic strength among these available basic sites in $MgAlO_x$ and Mg_3AlO_x, however, are comparable to that observed in pure MgO, with exchange rate constants at the maximum distributions of about 1.4×10^{-2} s^{-1} (Figure 15). This suggests that the existence of separate domains of MgO and Al_2O_3 in $MgAlO_x$ and Mg_3AlO_x samples. Only surface MgO contributed to the number of measured basic sites. The basic site density, however, was calculated based on the total surface area (MgO + Al_2O_3). This leads to lower basic site density without any effect on the strength distribution of basic sites related to MgO. Based on the $^{13}CO_2/^{12}CO_2$ isotopic exchange results, one can conclude that MgO and Al_2O_3 exist in separate phase, i.e., no solid solution formed in $MgAlO_x$ and Mg_3AlO_x samples. Both basic site density and strength in Mg_5AlO_x, however, was lower compared to MgO, suggesting the presence of AlO_x decreases the basicity of MgO possibly due to the formation of a Mg-Al-O solid solution.

Task 5: Bench Scale Testing at Air Products and Chemicals

Activities during this reporting period include meeting with Dr. Bernard A. Toseland from Air Products and Chemicals.

Staffing Plans

No changes.

Other activities

Two manuscripts *"Isobutanol and Methanol Synthesis of Copper Catalysts Supported on Modified Magnesium Oxide"* (M. Xu, M.J.L. Gines, B.L. Stephens and E. Iglesia) to be submitted to the Journal of Catalysis and *"Isotopic Switch Methods for the Characterization of Basic Sites in Modified MgO Catalysts"* (M. Xu, M.J.L. Gines and E. Iglesia) to be submitted to the Journal of Physical Chemistry are in the final draft and will be submitted for publication during the next reporting period.

REFERENCES:

1. Apesteguia, C.R., Soled, S.L., Miseo, S., U.S. Patent No. 5,387,570. Issued Feb. 7, 1995 to Exxon Research & Engineering Co., Florham Pk., N.J.
2. Slaa, J.C., van Ommmen, J.G. and J.R.H. Ross, *Catal. Today* **15** (1992) 129.
3. Sofianos, A., *Catal. Today* **15** (1992) 149.
4. Vedage, G.A., Himelfarb, P.B., Simmons, G.W. and K. Klier, *ACS Symp. Ser.* **279** (1985) 295.
5. Elliot, D.J. and F. Penella, *J. Catal.* **119** (1989) 359.
6. Ai, M., *Bull Chem. Japan* **64**(4) (1991) 1342.

7. Ai, M., *J. Catal.* **50** (1977) 291.
8. Luy, J.C., and Parera, J.M., *Appl. Catal.* **26**, 295 (1986).
9. Pines, H., and Manassen, J., *Adv. Catal.* **16**, 49 (1966).
10. Radlowski, C.A., and Hagen, G.P., U.S. Patent No 5,159,125, assigned to Amoco Corporation, Chicago, Ill.
11. Radlowski, C.A., and Hagen, G.P., U.S. Patent No 5,095,156, assigned to Amoco Corporation, Chicago, Ill.
12. King, D.S., and Nix, R.M., *J. Catal.*, **160,** 76 (1996).
13. Iglesia, E. and Boudart, M., *J. Catal.* **81,** 204 (1983).
14. Narita, K., Takeyawa, N., and Toyoshima, I., *React. Kinet. Catal. Lett.* **19,** (1982).
15. Boudart, M., and Djega-Mariadassou, G., "*Kinetics of Heterogeneous Catalytic Reactions*", Princeton Univ. Press, Princeton, N.J. (1984).
16. DePontes, M., Yokomizo, G.H., and Bell, A.T., *J. Catal.* **104,** 147 (1987).
17. McKenzie, A.L., Fishel, C.T., and Davis, R.J., *J. Catal.*, **138**, 547 (1992).
18. Kurokawa, H., Kato, K., Kuwabara, T., Ueda, W., Morikakawa, Y., Moro-Oka, Y., and Ikawa, T., *J. Catal.*, **126**, 208-218 (1990).
19. Pacchioni, G., Ricart, J.M., and Illas, F., *J. Am. Chem. Soc.*, **116**, 10152-8 (1994).
20. Krylov., O.V., "*Catalysis by Nonmetals*", Academic Press, New York and London, 1970).
21. Malinowsky S., Szczepanska S., and Sloczynski, J., *J. Catal.*, **7**, 67 (1967).
22. Choudhary, V.R., Rane, V.H., Catal. Lett., **4**, 101-106 (1990).
23. Reichle, W.T., *J. Catal.*, **94**, 547 (1985).
24. Schaper, H., Berg-Slot, J.J., and Stork,W.H.J., *Appl. Catal*, **54,** 79-90 (1989).
25. Shen, J., Cortright, R.D., Chen, Y., and Dumesic, J.A., *J. Phys. Chem.*, **98**, 8067 (1994).

4. PARTICIPATING PROJECT PERSONNEL

Mingting Xu
Postdoctoral Fellow

Marcelo J. L. Gines
Postdoctoral Fellow

Anne-Mette Hilmen
Postdoctoral Fellow

Zhengjie Hu
Undergraduate Researcher

Bernard A. Toseland
Sub-Contractor
Air Products and Chemicals

Enrique Iglesia
Principal Investigator

DOE F 1332.3
(11-84)

U.S. DEPARTMENT OF ENERGY
MILESTONE SCHEDULE ☐ PLAN ☒ REPORT

FORM APPROVED
OMB 1901-1400

1. TITLE	2. REPORTING PERIOD	3. IDENTIFICATION NUMBER
ISOBUTANOL METHANOL MIXTURE FROM SYNGAS	July 1, 1996-September 30, 1996	DE - AC22 - PC94PC066

4. PARTICIPANT NAME AND ADDRESS	5. START DATE	6. COMPLETION DATE
Department of Chemical Engineering University of California - Berkeley	Oct 1994	Sept 1997

7. ELEMENT CODE	8. REPORTING ELEMENT	9. DURATION	10. PERCENT COMPLETE a Plan	10. PERCENT COMPLETE b Actual
		94 → 95 → 96 → 97 O N D Q2 Q3 Q4 O N D J F M A M J J A S Q1 Q2 Q3 Q4		
	Task 4	Identify reaction intermediates by TPSR and high pressure infrared methods	60	40
	Tasks 3 & 5	Identify catalysts with highest isoalcohol yields (two) and evaluate at conditions resembling envisioned commercial practice.	60	30
	Task 5	Assess economic viability of these catalytic materials	30	0
	Task 5	Complete testing of at least two selected catalysts in slurry reactors.	30	0
	Tasks 3 & 5	Choose two materials for detailed studies of the reaction mechanism and of optimum synthetic protocols	0	0
	Tasks 3 & 5	Complete mechanistic studies on most promising materials	0	0
	Tasks 2 & 5	Develop synthetic procedures that can be carried out on a commercial scale Suggest a range of catalyst compositions for future study.	0	0
	Task 5	Complete testing of the two selected catalytic materials	0	0
	Task 5	Assess future research requirements, technical readiness and economic viability of the most promising approach	0	0
		Produce final report	0	0

DOE F 1332.3
(11-84)

U.S. DEPARTMENT OF ENERGY
MILESTONE SCHEDULE ☐ PLAN ☒ REPORT

FORM APPROVED
OMB 1901-1400

1. TITLE	2. REPORTING PERIOD	3. IDENTIFICATION NUMBER
ISOBUTANOL METHANOL MIXTURE FROM SYNGAS	July 1, 1996 - September 30, 1996	DE - AC22 - PC94PC066

4. PARTICIPANT NAME AND ADDRESS	5. START DATE	6. COMPLETION DATE
Department of Chemical Engineering University of California - Berkeley	Oct 1994	Sept 1997

7. ELEMENT CODE	8. REPORTING ELEMENT	9. DURATION	10. PERCENT COMPLETE a Plan	10. PERCENT COMPLETE b Actual
		94 — 95 — 96 — 97 O N D Q2 Q3 Q4 O N D J F M A M J J A S Q1 Q2 Q3 Q4		
	Task 3	Complete design, construction and start-up of packed bed reactor module	100	100
	Task 2	Prepare Cu-based catalyst compositions and characterize structure, surface area, and effectiveness of several synthetic approaches	100	100
	Task 2	Choose four promising materials for catalyst evaluation	100	100
	Task 3	Construct recirculating reactor module Establish reaction pathways and rate-determining steps	100	100
	Tasks 2 & 3	Identify catalyst components necessary to catalyze rate-determing steps that have been determined	100	100
	Tasks 2 & 3	Identify synthetic techniques to increase the reactivity and accessibility of such required sites	100	100
	Task 4	Complete construction and start-up of temperature programmed surface reaction apparatus and design of high-pressure infrared cell	100	100
	Task 4	Design and construction of high-pressure infrared cell	100	100
	Task 4	Calibrate between UCB and APCI laboratories by testing two selected catalysts in slurry reactors	100	20
	Task 2	Determine the density and reactivity of the required sites and implement synthetic methods to improve them	75	75

1. TITLE	2. REPORTING PERIOD	3. IDENTIFICATION NUMBER
ISOBUTANOL- METHANOL MIXTURE FROM SYNGAS	July 1, 1996 to Set. 30, 1996	DE-AC22-PC94PC066
2. PARTICIPANT NAME AND ADDRESS Department of Chemical Engineering University of California- Berkeley, Berkeley, CA 94720	5. COST PLAN DATE Oct. 15, 1996	6. START DATE OCT 1994 7. COMPLETION DATE OCT 1997

8. Element code	9. Reporting element	ACCRUED COSTS				ESTIMATED ACCRUED COSTS							12. Total contract Value	13. Variance
		Reporting period		Cumulative to date		a.total this fiscal year	b. balance of fiscal year	c. FY96 (1)	d. FY 97 (2)	(3)		e. total		
		a. Actual	b. Plan	c. Actual	d. Plan									
	1. Total (Direct material)	6,870	22,777	75,896	165,152	51,104	40,004	91,109	94,782			210,683	259,929	49,246
	a) Purchased Parts	6,870	9,106	65,995	110,468	42,427	-6,002	36,425	40,200			100,193	98,175	-2,018
	b) Subcontracted Items	0	13,670	3,970	128,722	3,970	50,709	54,679	54,582			109,261	161,754	52,493
	c) Other	0	0	5,931	74,043	4,708	0	0	0			5,931	0	-5,931
	2. Material Overhead	0	0	0	0	0	0	0	0			0	0	0
	3. Direct Labor 'Total	16,662	20,892	110,644	163,921	64,023	19,546	83,569	92,812			223,003	256,725	33,722
	4. Labor Overhead	0	0	0	0	0	0	0	0			0	0	0
	5. Fringe Benefits	1,707	3,350	12,626	26,168	7,300	6,099	13,400	15,368			34,093	41,538	7,445
	6. Special Testing	330	0	2,711	0	1,145	0	0	0			2,711	0	-2,711
	7. Special Equipment	2,168	2,000	290,137	260,000	45,958	-37,958	8,000	0			252,178	260,000	7,822
	8. Travel	1,036	1,629	6,918	12,720	4,731	1,784	6,515	7,020			15,723	19,740	4,017
	9. Consultants	0	0	0	0	0	0	0	0			0	0	0
	10. Other Direct costs	0	6,114	0	47,745	0	24,455	24,455	25,677			50,132	73,422	23,290
	11. Direct costs and Overhead	28,773	56,761	498,932	675,702	174,261	52,783	227,044	235,653			787,368	911,354	123,986
	12. General and Administrative Expense '49.5 %	13,276	20,505	104,077	165,757	64,023	17,997	82,020	90,358			212,431	256,108	43,677
	13. Facilities Capital Cost of Money	0	0	0	0	0	0	0	0			0	0	0
	14. Total Estimated Cost	42,049	77,266	603,009	841,457	238,284	70,778	309,062	326,008			999,795	1,167,462	167,667
	15. Fee	0	0	0	0	0	0	0	0			0	0	0
	16. Cost Sharing	0	9,949	205,766	252,851	17,011	22,786	39,797	56,789			285,341	301,651	16,310
	17. Total estimated DOE funds spent = Item 14-Item 16	42,049	67,316	397,243	588,606	221,273	47,992	269,265	269,219			714,454	865,811	151,357
14. Total		42,049	67,316	397,243	588,606	221,273	47,992	269,265	269,219			714,454	865,811	151,357

15. DOLLARS EXPRESSED IN	16. SIGNATURE OF PARTICIPANT PROJECT MANAGER AND DATE	17. SIGNATURE OF PARTICIPANT'S AUTHORIZED FINANCIAL SERVICE REPRESENTATIVE AND DATE
One U.S. Dollar		Lourdes S. Ferrer